EC
Journals.ASM.org

Regulation of Vacuolar H^+-ATPase Activity by the Cdc42 Effector Ste20 in *Saccharomyces cerevisiae*

Meng Lin,[a] Sheena Claire Li,[b] Patricia M. Kane,[b] and Thomas Höfken[a,c]

Institute of Biochemistry, Christian Albrechts University, Kiel, Germany[a]; Department of Biochemistry and Molecular Biology, SUNY Upstate Medical University, Syracuse, New York, USA[b]; and Division of Biosciences, Brunel University, West London, United Kingdom[c]

In the budding yeast *Saccharomyces cerevisiae*, the Cdc42 effector Ste20 plays a crucial role in the regulation of filamentous growth, a response to nutrient limitation. Using the split-ubiquitin technique, we found that Ste20 forms a complex with Vma13, an important regulatory subunit of vacuolar H^+-ATPase (V-ATPase). This protein-protein interaction was confirmed by a pull-down assay and coimmunoprecipitation. We also demonstrate that Ste20 associates with vacuolar membranes and that Ste20 stimulates V-ATPase activity in isolated vacuolar membranes. This activation requires Ste20 kinase activity and does not depend on increased assembly of the V_1 and V_0 sectors of the V-ATPase, which is a major regulatory mechanism. Furthermore, loss of V-ATPase activity leads to a strong increase in invasive growth, possibly because these cells fail to store and mobilize nutrients efficiently in the vacuole in the absence of the vacuolar proton gradient. In contrast to the wild type, which grows in rather small, isolated colonies on solid medium during filamentation, hyperinvasive *vma* mutants form much bigger aggregates in which a large number of cells are tightly clustered together. Genetic data suggest that Ste20 and the protein kinase A catalytic subunit Tpk2 are both activated in the *vma13*Δ strain. We propose that during filamentous growth, Ste20 stimulates V-ATPase activity. This would sustain nutrient mobilization from vacuolar stores, which is beneficial for filamentous growth.

The Rho-type GTPase Cdc42 regulates cell morphology and signal transduction in eukaryotic cells (11, 17, 40). In the budding yeast *Saccharomyces cerevisiae*, the p21-activated kinase Ste20 is one of the best-characterized effectors of Cdc42 that triggers these pathways. Ste20 promotes polarized growth, exit from mitosis, and cell death (1, 16, 53). It also regulates vacuolar inheritance, mRNA decay, and the synthesis and uptake of sterols (2, 28, 29, 68). Furthermore, Ste20 activates distinct mitogen-activated protein kinase (MAPK) cascades that control filamentous growth, mating, and osmotic-stress responses (26, 30, 38, 44, 45, 49). Consistent with these functions, Ste20 can be found in the cytoplasm and at the plasma membrane at sites of polarized growth, including the bud cortex and tips of mating projections (25, 43).

Upon nutrient limitation, budding yeast cells can switch to filamentous growth (13, 49). This is characterized by cell elongation, a switch to unipolar budding, increased cell-cell adhesion, increased cell-substratum adhesion, and the ability to penetrate a solid medium, such as agar. Together, these mechanisms allow the cells to forage for nutrients. By mechanisms that are not fully understood, nutrient sensors trigger at least two signaling pathways: a MAPK module activated by Ste20 and a cyclic AMP (cAMP)-dependent protein kinase A (PKA) pathway. The nutrient sensors may relay their signal to Ras2, which activates a cascade that consists of Cdc42, Ste20, the MAPK kinase kinase Ste11, the MAPK kinase Ste7, and the MAPK Kss1 (Fig. 1) (30, 36, 49). In addition, Ras2 activates the adenylate cyclase Cyr1, which stimulates cAMP production (Fig. 1) (59). Increased cAMP levels result in PKA activation by dissociating the inhibitory cAMP-binding regulatory subunit Bcy1 from the catalytic subunits Tpk1, Tpk2, and Tpk3 (60, 61). Tpk2 is an important activator of filamentation, whereas Tpk1 and Tpk3 function as inhibitors (39, 50). It has also been reported that nutrient sensors may activate the MAPK cascade and the PKA pathway independently of Ras2 (33, 42, 65). Stimulation of the filamentous-growth MAPK cascade by the plasma membrane-bound Sho1-Msb2 complex, for instance, does not seem to involve Ras2 (5). In addition to the MAPK and PKA pathways, the 5′-AMP-dependent kinase Snf1 is involved in filamentation, as well (4, 24).

Vacuolar H^+-ATPases (V-ATPases) are ATP-driven proton pumps that acidify organelles, such as the lysosome, the Golgi apparatus, and endosomes, in all eukaryotic cells (12, 21). Acidification of the lysosome-like vacuole in budding yeast is implicated in metabolite storage, autophagy, and ion homeostasis (27). The electrochemical gradient established by the V-ATPase is exploited by numerous secondary transporters, and the acidic vacuolar pH is optimal for proteolysis of proteins arriving by autophagy or endocytosis. As a result, the vacuole is well suited for storage of nutrients when they are plentiful and for mobilization during periods of depletion (67). The importance of V-ATPases in the plant tonoplast for nutrient storage was recently highlighted by the discovery that the vacuolar subunit isoforms of the *Arabidopsis* V-ATPase are essential for nutrient storage (23).

The V-ATPase is a membrane-bound multisubunit enzyme complex composed of two distinct domains (12, 21). The V_1 sector, which resides on the cytoplasmic side of the membrane, hydrolyzes ATP and contains 8 different subunits, whereas the membrane-embedded V_0 sector, which is composed of 6 different subunits, translocates protons across the membrane. Among eukaryotes, V-ATPases are highly conserved in both their overall structure and the sequences of individual subunits. V-ATPase activity is tightly regulated. A major regulatory mechanism is the

Received 23 December 2011 **Accepted** 2 February 2012
Published ahead of print 10 February 2012
Address correspondence to Thomas Höfken, thomas.hoefken@brunel.ac.uk.
M. Lin and S. C. Li contributed equally to this work.

doi:10.1128/EC.05286-11

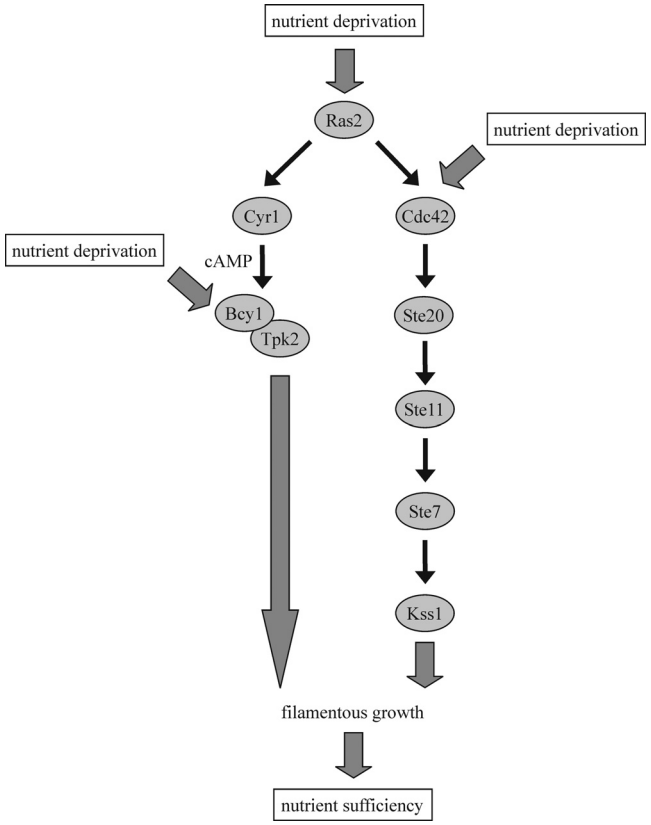

FIG 1 The MAPK and PKA pathways in filamentation. See the text for details. The precise molecular signaling mechanisms are not clear. In addition to the activation of the filamentous-growth MAPK and PKA pathways by Ras2, as shown here, it has been reported that these branches can be stimulated in a Ras2-independent manner, as well. Our data suggest that the loss of V-ATPase activity in *vma* mutants strongly stimulates both Ste20 and Tpk2, probably because these cells are unable to efficiently store and mobilize nutrients in vacuoles.

dissociation of V-ATPase into its V_0 and V_1 sectors. In budding yeast, glucose depletion induces rapid and reversible V-ATPase disassembly (20). This process is regulated in part by the Ras/cAMP/PKA pathway (3), whereas a heterotrimeric complex termed RAVE is required for reassembly of V-ATPase complexes (52, 55). Other proteins, including glycolytic enzymes, such as aldolase, have also been implicated in regulated dissociation of V-ATPases (32). Recently, Dechant et al. (6) proposed that a decrease in cytosolic pH, which is a consequence of glucose starvation, triggers V-ATPase disassembly. The dissociated V_0 and V_1 sectors are both inactive (41, 69). This inactivation is critical, in particular, for the V_1 sector, because release of an uncoupled ATPase into the cytosol could deplete cellular energy stores. Vma13, the V-ATPase subunit H, plays an important role in silencing ATP hydrolysis by the V_1 sector. Cytosolic V_1 complexes from cells lacking *VMA13* have significant ATPase activity, and this activity can be silenced by addition of bacterially expressed H subunit (41, 7). Vma13 is also the only subunit that is not required for the full assembly of V-ATPase. In the absence of *VMA13*, V_0-V_1 complexes assemble and are transported to the vacuole, but these complexes are inactive (15). These results suggest that Vma13 functions as an activator in the fully assembled V-ATPase and an inhibitor of detached V_1 sectors.

In this work, we show evidence for Ste20 binding to Vma13 and for localization of Ste20 at vacuolar membranes. We also find that Ste20 positively regulates V-ATPase activity *in vivo*, and this activation is independent of V-ATPase assembly. Furthermore, deletion of *VMA13* or other V-ATPase subunits leads to a strong increase in agar invasion, possibly due to defective nutrient storage and mobilization in these cells. We propose that during filamentous growth, Ste20 not only triggers a MAPK cascade, but, in parallel, activates the V-ATPase, facilitating mobilization of intracellular nutrient reserves.

MATERIALS AND METHODS

Yeast strains, plasmids, and growth conditions. All yeast strains used in this study are listed in Table 1. The strains are in the Σ1278b background (PPY966), with the exception of strains used for vacuolar assays. For vacuole isolation, wild-type SF838-5Aα was used. Yeast strains were constructed using PCR-amplified cassettes (18, 31) and were grown in 1% yeast extract, 2% peptone, 2% dextrose (YPD) or synthetic complete (SC) medium. For induction of the *GAL1* promoter, yeast cells were grown in YP medium with 3% raffinose instead of glucose. Galactose (final concentration, 2%) was added to induce the *GAL1* promoter. To compare the growth rates between strains, cells were grown overnight in liquid YPD medium. Serial dilutions starting from 10^4 cells were then spotted on YPD plates and incubated at 30°C for 2 days.

All constructs used in this work are listed in Table 2. To obtain 2μm plasmids containing *STE20-3HA* and *STE20*^{K649A}*-3HA* under the control of the *STE20* promoter, a C-terminal *STE20-3HA* fragment was amplified by PCR using pRS316-pGAL1-*STE20-3HA* and pRS316-pGAL1-*STE20*^{K649A}-3HA, respectively, as templates and the following primers: 5′-TCCTCCGTCGACAAGTGA and 5′-ATGCGGGCCCAACAGCTAT GACCATGAT. PCR products were digested with SalI and ApaI and ligated into SalI/ApaI-cut pRS425-*STE20*.

Split-ubiquitin technique. The split-ubiquitin screen using *STE20* as bait is described by Tiedje et al. (57). For the interaction assays, 10^4 cells carrying the split-ubiquitin plasmids were spotted on SC medium lacking histidine and leucine to select for the plasmids or onto SC medium lacking histidine and leucine and supplemented with 0.5 g/liter 5-fluoroorotic acid (5-FOA) to monitor protein interactions. The 5-FOA plates also

TABLE 1 Yeast strains used in this study

Name	Genotype	Source or reference
MLY65	PPY966 *vma13*Δ::*His3MX6*	This study
MLY125	PPY966 *vma2*Δ::*His3MX6*	This study
MLY126	PPY966 *vma3*Δ::*His3MX6*	This study
MLY150	PPY966 *ste20*Δ::*hphNT1 vma2*Δ::*His3MX6*	This study
MLY151	PPY966 *ste20*Δ::*hphNT1 vma3*Δ::*His3MX6*	This study
MLY159	PPY966 *tpk2*Δ::*His3MX6*	This study
MLY161	PPY966 *tpk2*Δ::*His3MX6 ste20*Δ::*hphNT1*	This study
MLY166	PPY966 *tpk2*Δ::*klTRP1 vma13*Δ::*His3MX6*	This study
MLY167	PPY966 *tpk2*Δ::*klTRP1 ste20*Δ::*hphNT1 vma13*Δ::*His3MX6*	This study
MLY168	PPY966 *vma13*Δ::*His3MX6 ste7*Δ::*klTRP1*	This study
MLY170	PPY966 *ste20*Δ::*His3MX6 vma13*Δ::*hphNT1*	This study
MLY177	PPY966 *vma13*Δ::*His3MX6 ste11*Δ::*klTRP1*	This study
MLY208	PPY966 *STE20-3HA-His3MX6*	This study
PPY966	*MAT***a** *his3*::*hisG leu2*::*hisG trp1*::*hisG ura3-52*	57
SHY26	PPY966 *ste11*Δ::*His3MX6*	This study
SHY45	PPY966 *ste7*Δ::*His3MX6*	This study
THY697	PPY966 *ste20*Δ::*hphNT1*	58

TABLE 2 Plasmids used in this study

Name	Genotype	Source or reference
pAK6	pADNX carrying *pADH1-NUbiquitin-VMA13*	This study
pCT44	pADNX carrying *pADH1-NUbiquitin-EXO70*	This study
pKA86	pRS316 carrying *pGAL1-STE20-3HA*	57
pKK19	pRS316 carrying *myc-VMA13*	41
pTH197	pRS313 carrying *pMET25-STE20-CUbiquitin-RURA3*	57
pTH263	pRS425 carrying *STE20*	This study
pTH380	pRS425 carrying *STE20-3HA*	This study
pTH381	pRS425 carrying *STE20^{K649A}-3HA*	This study
pTH383	pADNX carrying *pADH1-NUbiquitin-VMA2*	This study
pTH385	pRS313 carrying *pMET25-STE14-CUbiquitin-RURA3*	This study
pTH386	pADNX carrying *pADH1-NUbiquitin-VMA3*	This study
MBP-Vma13	pMALpAse carrying *VMA13*	7

lacked methionine and cysteine to induce expression of the *STE20* and *STE14* fusion genes under the control of the *MET25* promoter. The plates were grown for 2 days at 30°C.

Biochemical interaction of Vma13 and Ste20. Maltose-binding protein (MBP)-tagged Vma13 was expressed and purified from bacteria as described previously (7), but with the following modifications. Transformed cells were grown to an A_{600} of 1 at 30°C. These cultures were then saved as frozen 1-ml stocks in 50% glycerol at −80°C, and 1 ml of frozen stock culture was added to 1 liter of LB containing 125 μg/ml ampicillin and 2 g glucose to grow the cells for MBP-Vma13 purification. The soluble fraction from the bacterial cell lysate was bound to a suspension of amylose resin (New England BioLabs), and the resin was washed with at least 20 volumes of cold TBSE (20 mM Tris-HCl, pH 7.2, 150 mM NaCl, 0.5 mM EDTA). Purified MBP-Vma13 was eluted in five 1-ml washes of TBSE containing 100 mM maltose.

Ste20-hemagglutinin (HA) was isolated from wild-type cells transformed with the plasmid pKA86 carrying HA-tagged *STE20* under the control of the *GAL1/10* promoter after 3 h of galactose induction. The cells were lysed, and cytosolic fractions were prepared as described previously (56). Each sample was incubated with 100 μl of protein A-Sepharose beads (a 40% suspension in phosphate-buffered saline-bovine serum albumin [PBS-BSA]) and 100 μg of anti-HA antibody (monoclonal antibody 16B12 from Covance Research Products) at 4°C for 1 h. Transformed cells that were not induced with galactose were treated in parallel as a negative control. The beads were washed with lysis buffer (50 mM Tris-HCl, 30 mM KCl, 30 mM NaCl, 0.3 mM EDTA) three times. Purified MBP-Vma13 was then incubated with Ste20-HA-bound beads (or beads from the uninduced control) at 4°C with gentle shaking for 3 h. The beads were washed three times with TBSE, and then the bound protein was eluted, separated by SDS-PAGE, and transferred to nitrocellulose as described previously (7). The level of MBP-Vma13 bound to the beads was detected on immunoblots with anti-MBP antibody (New England BioLabs).

For the coimmunoprecipitation experiment, 200 ml *STE20-3HA* cells carrying either pRS316-myc-VMA13 (pKK19) or the empty pRS316 were grown to an A_{600} of 1. Cells were harvested, washed twice with PBS, and resuspended in 10 ml PBS. DSP (dithiobis [succinimidylpropionate]) was added from a freshly prepared 20 mM stock solution in dimethyl sulfoxide (DMSO) to a final concentration of 1 mM. The reaction mixture was incubated for 30 min at room temperature. The reaction was stopped by adding Tris, pH 7.5, to a final concentration of 20 mM and incubation for 15 min at room temperature. After washing with lysis buffer (20 mM Tris, pH 7.5, 100 mM NaCl, 10 mM EDTA, 1 mM EGTA, 5% glycerol, 1% Triton X-100), the cells were disrupted with glass beads in lysis buffer and clarified by centrifugation at 13,000 rpm for 5 min. The protein concentration was determined using Bradford protein assay solution. myc-Vma13 was immunoprecipitated by adding mouse monoclonal anti-myc antibody (9E10; Santa Cruz Biotechnology) and protein G-Sepharose (GE Healthcare). The resin was washed three times with lysis buffer, resuspended in 2× SDS sample buffer, and analyzed by immunoblotting. Mouse monoclonal anti-HA (12CA5) was obtained from Roche Diagnostics, and secondary antibodies were from Jackson ImmunoResearch Laboratories.

Filamentation assays. For agar invasion assays, 10^4 cells of an overnight YPD culture were spotted on a YPD plate and grown for 3 days at 30°C. The plates were photographed before and after being rinsed under a stream of deionized water.

For the single-cell invasive-growth assay, cells were grown to stationary phase in SC medium, washed twice with water, and spread onto synthetic complete medium lacking glucose at a concentration of 10^4 cells/plate. The plates were incubated at 30°C for 18 h and analyzed microscopically with a Zeiss Axiovert 200 M fluorescence microscope. Images were captured using a Zeiss AxioCam MRm charge-coupled-device (CCD) camera.

The formation of cell clusters was analyzed by spotting 10^3 cells of an overnight YPD culture on a YPD plate and incubating the plate for 3 days at 30°C. The strains were examined microscopically after the plates were washed with water.

Vacuole isolation and biochemical analysis. Wild-type (SF838-5Aα) cells or the congenic *ste20Δ::kanMX* strain were transformed with a multicopy plasmid carrying *STE20*, *STE20-3HA*, or *STE20^{K649A}-3HA* (*STE20^{KD}-3HA*). The cells were grown to log phase in SC buffered to pH 5 with 50 mM morpholineethanesulfonic acid (MES), converted to spheroplasts, and lysed, and then vacuolar vesicles were isolated by Ficoll density gradient centrifugation as described previously (48). ATPase activity was determined by coupled enzyme assay, and activity sensitive to 100 nM concanamycin A was taken as V-ATPase activity (48). For immunoblot analysis, vacuolar vesicles were solubilized, separated by SDS-PAGE, and transferred to nitrocellulose as described previously (56). V-ATPase subunits were detected with mouse monoclonal antibodies 10D7 (anti-V_0 a subunit), 8B1 (anti-V_1 A subunit), 13D11 (anti-V_1 B subunit), and 7 A2 (anti-V_1 C subunit) (22). *STE20-HA* and *STE20^{KD}-3HA* were detected with monoclonal antibody 16B12 (Covance). Activities were compared between strains using the two-sample *t* test assuming equal variance in Microsoft Excel.

RESULTS

Ste20 interacts with the V-ATPase subunit Vma13. In an effort to identify regulators and targets of Ste20, we screened for proteins that bind to Ste20 using the split-ubiquitin system (57). This technique is based on the ability of the N- and C-terminal halves of ubiquitin to form a native-like ubiquitin (Fig. 2A) (19). Ubiquitin-specific proteases present in the cytosol and nucleus recognize the reconstituted ubiquitin, but not its halves, and cleave off a reporter protein, which had been linked to the C-terminal half of ubiquitin. The assay described here employs RUra3, a modified Ura3 with an arginine as the first amino acid, as the reporter (63). The freed RUra3 is rapidly degraded because arginine is a destabilizing residue in the N-end rule pathway. Therefore, interaction between two proteins fused to the N- and C-terminal halves of ubiquitin, respectively, results in nongrowth on medium lacking uracil. Conversely, growth on 5-FOA medium indicates a protein-protein interaction because 5-FOA is converted by Ura3 into a toxic compound. Using this technique, we identified the V-ATPase subunit Vma13 as an interactor of Ste20 (Fig. 2B). Ste20 does not bind to either Vma2, a component of the V_1 domain, or the V_0 subunit Vma3 in this assay, indicating that the observed Ste20-Vma13 interaction is specific (Fig. 2B).

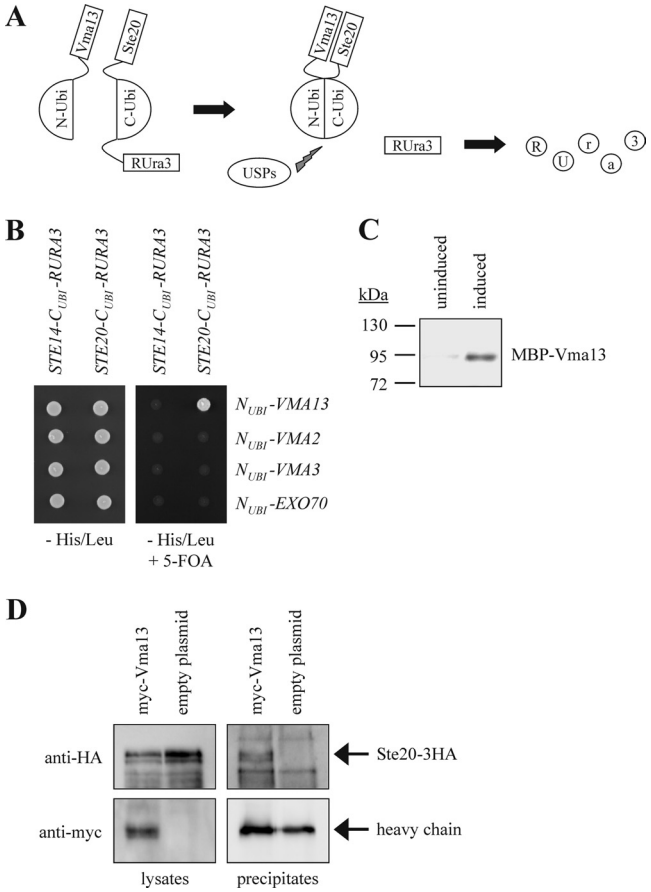

FIG 2 Ste20 binds to Vma13. (A) The split-ubiquitin system. The N-terminal and C-terminal halves of ubiquitin (N-Ubi and C-Ubi) alone do not assemble. If Vma13, fused to N-Ubi, binds to Ste20, linked to C-Ubi, the two halves of ubiquitin are brought into close proximity. This reconstituted quasinative ubiquitin is recognized by ubiquitin-specific proteases (USPs), which cleave off the reporter RUra3, which is fused to Ste20. The released RUra3, a modified version of the enzyme Ura3 with an arginine at the extreme N terminus, is targeted for degradation by the enzymes of the N-end rule. Since Ura3 converts 5-FOA to the toxic 5-fluorouracil, 5-FOA resistance indicates an interaction between Ste20 and Vma13. (B) Ste20 interacts with Vma13 using the split-ubiquitin system. Cells (10^4) of the indicated plasmid combinations were spotted either onto medium lacking histidine and leucine to select for the plasmids or onto medium lacking histidine and leucine and supplemented with 5-FOA to monitor protein interactions. The unrelated genes *STE14* and *EXO70* served as negative controls. (C) Ste20 interacts with Vma13 in a pulldown assay. Wild-type cells were transformed with a plasmid carrying 3HA-tagged *STE20* (*STE20-3HA*) under the control of the *GAL1/10* promoter. Transformed cells were grown in raffinose medium to relieve glucose repression and either left in raffinose (uninduced) or transferred to galactose medium (induced) for 3 h. Ste20-HA was immunoprecipitated from yeast cell lysate with anti-HA antibody, followed by protein A-Sepharose. MBP-tagged Vma13 purified from *E. coli* was added directly to the immunoprecipitates on protein A-Sepharose. After incubation and washing of the beads to remove unbound protein, binding was assessed by SDS-PAGE and immunoblotting with anti-MBP antibody. (D) Ste20 binds to Vma13 *in vivo*. *STE20-3HA* cells carrying either a pRS316 plasmid with myc-*VMA13* or the empty pRS316 were lysed, and equal amounts of protein extract were precipitated with anti-myc antibodies. The immunoprecipitates were analyzed by immunoblotting using antibodies against the HA and myc epitopes, respectively. myc-Vma13 runs at the same height as the heavy chain. However, a stronger signal indicates that the protein was precipitated.

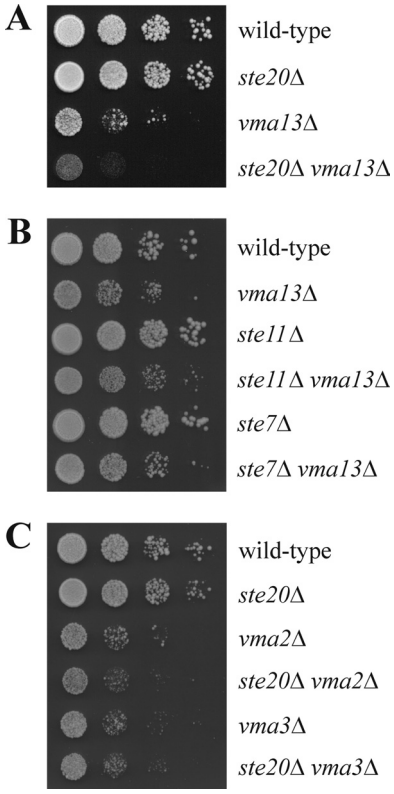

FIG 3 Genetic interaction between *STE20* and *VMA13*. (A) *STE20* deletion exacerbates the growth defect of *vma13*Δ cells. Serial dilutions (1:10) of the indicated strains were spotted on YPD and incubated for 2 days at 30°C. (B) Deletion of *STE11* and *STE7*, respectively, does not affect the growth rate of the *vma13*Δ strain. Growth was assessed by serial dilutions as in panel A. (C) *STE20* does not interact genetically with *VMA2* or *VMA3*. Growth was assessed by serial dilutions as in panel A.

To confirm the protein-protein interaction between Ste20 and Vma13 by an independent approach, Ste20-3HA was expressed from the inducible *GAL1/10* promoter and immunoprecipitated from a yeast cell lysate. The immunoprecipitates bound to protein A-Sepharose beads were incubated with MBP-Vma13 purified from *Escherichia coli*. In this assay, MBP-Vma13 was specifically pulled down by Ste20-3HA in an induced sample but was not bound to the beads in an uninduced sample (Fig. 2C).

Finally, binding of HA-tagged Ste20 to myc-tagged Vma13 was confirmed by immunoprecipitation from yeast cells using anti-myc antibodies. Ste20-3HA coprecipitated with myc-Vma13 but was not detected in immunoprecipitated protein from cells that do not express myc-Vma13 (Fig. 2D). Thus, Ste20 forms a complex with Vma13 *in vivo*.

We next analyzed genetic interactions between *STE20* and *VMA13*. As shown previously, the growth rate of *vma13*Δ cells was reduced in comparison to the wild type (Fig. 3A) (15). Notably, additional deletion of *STE20* in the strain exacerbated this growth defect (Fig. 3A), suggesting that *STE20* and *VMA13* act in parallel to support normal cell growth. In contrast, there is no synthetic growth defect between *vma13*Δ and *ste11*Δ and *ste7*Δ, two mutants in the filamentation and pheromone response MAPK pathways activated by Ste20 (Fig. 1 and 3B). We also examined genetic interactions between *STE20* and the V-ATPase subunit genes *VMA2* and *VMA3*. Deletion of either *VMA2* or *VMA3* resulted in

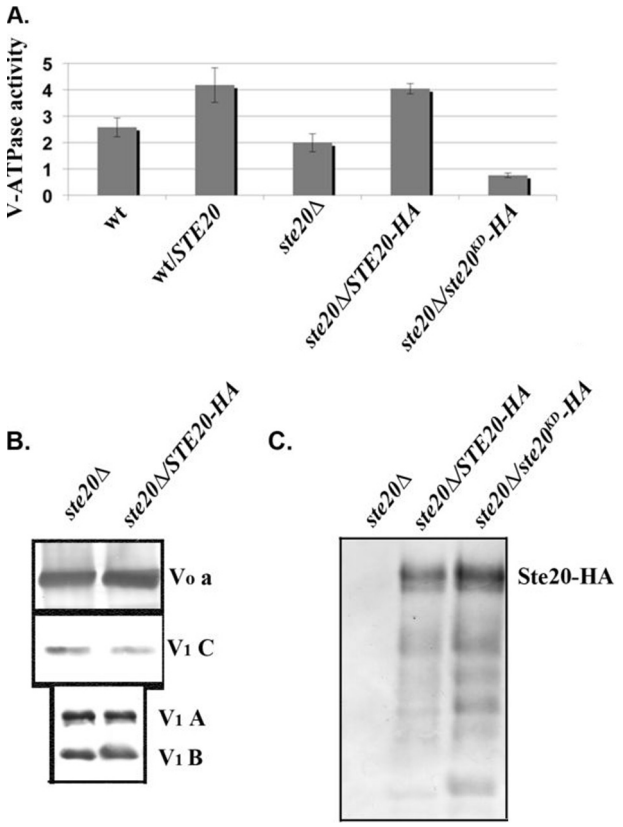

FIG 4 Ste20 localizes to the vacuole and activates V-ATPase activity. (A and B) Vacuolar vesicles were isolated from wild-type cells, wild-type cells transformed with a multicopy plasmid expressing *STE20* from its native promoter (wt/*STE20*), a *ste20*Δ mutant, and the *ste20*Δ mutant transformed with a multicopy plasmid bearing either 3HA-tagged *STE20* (*STE20-HA*) or a 3HA-tagged kinase-dead mutant of *STE20* (*ste20^{KD}-HA*). (A) Concanamycin A-sensitive ATPase activity in the isolated vacuolar vesicles is expressed as μmol ATP hydrolyzed/min/mg vacuolar protein. For each sample, the mean ± standard error of the mean (SEM) for four to seven independent vacuolar preparations is shown. (B) Vacuolar vesicles from the *ste20*Δ and *STE20-3HA*-overexpressing cells were solubilized, and equivalent quantities of vacuolar protein were separated by SDS-PAGE and transferred to nitrocellulose, followed by immunoblotting with antibodies to subunit a of the V-ATPase V_0 sector and subunits A, B, and C of the V-ATPase V_1 sector. (C) Localization of wild-type and kinase-dead HA-tagged Ste20 to vacuolar membranes. Equal concentrations of vacuolar protein were separated by SDS-PAGE as in panel B and then probed for the presence of Ste20-HA on immunoblots. The predicted molecular mass of Ste20-3HA is indicated.

a growth defect comparable to that of the *vma13*Δ strain. However, the loss of *STE20* in these strains had no effect on the growth rate (Fig. 3C). Thus, the genetic interaction between *VMA13* and *STE20* is remarkably specific.

Activation of V-ATPase by Ste20. Since Ste20 binds to Vma13, it is tempting to speculate that Ste20 regulates V-ATPase activity. To test this, we first isolated vacuolar vesicles from wild-type and *ste20*Δ cells and cells overexpressing *STE20* and assessed concanamycin A-sensitive ATPase activity. *STE20* expressed from its own promoter or the *GAL1/10* promoter is active, allowing assessment of its activity in the absence of triggers, such as nutrient deprivation (43, 64). As shown in Fig. 4A, the specific ATPase activity in vacuolar vesicles isolated from a *ste20*Δ strain was not significantly different from the activity in wild-type vacuolar vesicles ($P > 0.05$). Overexpression of *STE20* in the wild-type strain appeared to give higher ATPase activity, but the difference from wild-type activity was not statistically significant ($P = 0.14$). However, we also transformed *ste20*Δ cells with *STE20-3HA* and *STE20^{K649A}-3HA*, a kinase-dead allele of Ste20 (64), and then isolated vacuolar vesicles. As shown in Fig. 4A, overexpressed *STE20-3HA* activates V-ATPase activity to an extent comparable to the untagged *STE20*; this activity was also significantly different from those of both the *ste20*Δ and wild-type strains ($P \leq 0.01$ for each strain). In contrast, the inactive *STE20^{KD}-3HA* does not activate the V-ATPase. We next asked whether differences in V-ATPase activity in the *ste20*Δ mutant and *STE20*-overexpressing strains could be accounted for by differences in V-ATPase subunit levels at the vacuole. Immunoblots of vacuolar vesicles from *ste20*Δ and *STE20-3HA*-overexpressing strains were probed for V_0 subunit a and V_1 subunits A, B, and C, as shown in Fig. 4B. There were no consistent differences in the levels of these subunits in the wild-type, *ste20*Δ, or *STE20*-overexpressing cells over several independent vacuole preparations. The ratio of V_1 to V_0 subunit levels at the vacuole provides an established measure of V-ATPase assembly (3, 8, 20), so these results also imply that Ste20 does not change V-ATPase activity by altering the level of V_1-V_0 assembly. The levels of alkaline phosphatase, a vacuolar membrane protein that is transported independently of the V-ATPase, also showed no significant differences (data not shown). In order to determine whether Ste20 is localized to the vacuole, we also probed immunoblots of vacuolar vesicles for Ste20-3HA (Fig. 4C). Both the wild-type Ste20-HA and the kinase-dead mutant *ste20^{K649A}-3HA* (*ste20^{KD}-HA*) are localized to vacuolar membranes, even though the kinase-dead mutant does not support activation of the V-ATPase. These results indicate that Ste20 kinase activity is required for V-ATPase activation and that the kinase could exert its activity at the vacuolar membrane.

Finally, we tested whether direct phosphorylation of Vma13 could account for the activation of V-ATPase activity by Ste20. However, although bacterially expressed Vma13 could bind to Ste20 in pulldowns, there was no phosphorylation of Vma13 under these conditions. As a result, we cannot yet directly attribute V-ATPase activation to direct phosphorylation by Ste20.

V-ATPase activity and filamentous growth. Since *STE20* and *VMA13* interact genetically and at the protein level, we examined whether the V-ATPase contributes to processes that are regulated by Ste20. *vma13*Δ cells have normal morphology and form a mating projection in response to pheromone (data not shown). We also examined invasive growth. For this assay, cells are spotted at very high density on the rich YPD medium. Under these conditions, nutrients are locally used up quickly. As a consequence, filamentation is induced and cells penetrate the agar. This agar invasion can easily be assessed by washing off cells that grow only superficially. In the absence of *VMA13*, cells exhibited a marked increase in agar invasion (Fig. 5A). Presumably, *vma13*Δ cells are unable to store and/or mobilize nutrients in the vacuole efficiently due to the lack of V-ATPase activity. Therefore, these cells might be more sensitive to nutrient deprivation. We next asked whether this phenotype was specific to *vma13*Δ cells or characteristic of a general loss of V-ATPase activity. Like the *vma13*Δ strain, *vma2*Δ and *vma3*Δ cells displayed a growth defect and a hyperinvasive phenotype (Fig. 5A). Therefore, increased agar invasion seems to be a common feature of cells lacking V-ATPase activity and is not specific to *vma13*Δ.

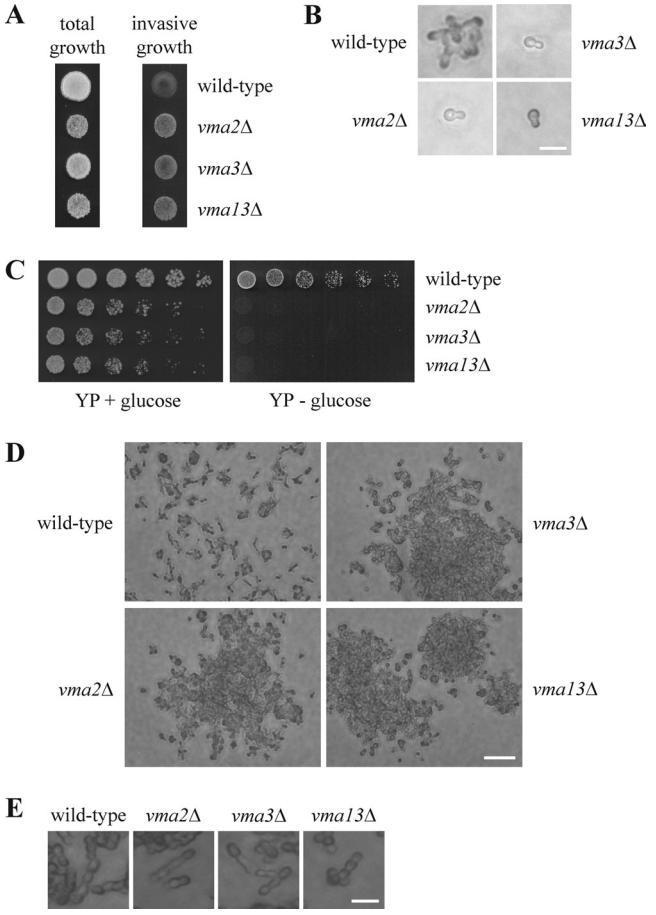

FIG 5 Cells lacking V-ATPase activity are hyperinvasive. (A) Deletion of V-ATPase subunits leads to stronger agar invasion. Cells (10^4) of the indicated strains were spotted on a YPD plate and grown for 3 days at 30°C. Photographs were taken before (total growth) and after (invasive growth) rinsing with water. Note that agar invasion by the *vma* mutants is markedly stronger than that by the wild type even though these strains have a greatly reduced growth rate. (B) *vma* mutants fail to form colonies in the absence of glucose. Cells (10^4) of the indicated strains were spread on SC medium lacking glucose and were incubated for 18 h at 30°C. Bar, 10 μm. (C) Cells lacking V-ATPase activity are unable to grow on YP medium lacking glucose. Serial dilutions (1:3) of the indicated strains were spotted on YP plates with or without glucose and incubated for 2 days at 30°C. (D) *vma* mutants form cell clusters in response to nutrient deprivation. Cells (10^3) of the indicated strains were spotted on a YPD plate and grown for 3 days at 30°C. Cells that did not invade the agar were washed off with water. Bar, 50 μm. (E) Morphology of cells grown on agar. The indicated strains were treated as described for panel D but incubated for 3 days at 30°C. Bar, 10 μm.

To examine the morphology of *vma* cells during filamentation, a single-cell invasive-growth assay was performed. For this experiment, cells were grown overnight in liquid SC medium supplemented with glucose. The cells were then washed to remove nutrients and spread onto SC plates lacking glucose. Under these conditions of very severe nutrient deprivation, wild-type cells undergo few divisions and form small colonies of branched and slightly elongated cells, presumably by utilizing stored nutrients (Fig. 5B) (4). In contrast, cells lacking *VMA2*, *VMA3*, or *VMA13* did not divide (Fig. 5B). Even after more than 48 h of incubation, we observed only single *vma* cells. This is clearly different from the growth of *vma* strains on rich medium, where growth is slowed but cells still divide. Therefore, the failure to form colonies cannot be explained by the reduced growth rate of these strains. Instead, this result is consistent with the notion that the *vma* strains are unable to store and mobilize nutrients efficiently. The complete loss of growth of *vma2*Δ, *vma3*Δ, and *vma13*Δ cells upon glucose removal is not restricted to SC medium. On YPD medium, growth of the *vma* mutants is reduced, whereas on YP medium lacking glucose, it is completely abolished (Fig. 5C). Even after several days, no growth of the *vma* mutants was observed.

The increased agar invasion of the *vma* mutants shown in Fig. 5A could be due to either stronger cell elongation or increased cell-cell adhesion and/or cell-substratum adhesion. Since *vma* strains did not form microcolonies on SC medium in the absence of glucose (Fig. 5B), we examined the morphology of cells grown on YPD plates. When cells were grown at a very high density, as shown in Fig. 5A, it was extremely difficult to make out individual cells. Therefore, we analyzed cells that were spotted on YPD agar at 1/10 of the normal density. Under these conditions, cells still penetrated the agar. After removing superficially growing cells by rinsing the plate, isolated small colonies were observed for the wild type (Fig. 5D). In contrast, *vma* mutants formed large cell clusters (Fig. 5D). These contained a much higher number of cells than the wild-type colonies, and the cells seemed to be densely packed together. Notably, these aggregates were not observed when *vma* strains were grown in liquid culture. Thus, it seems that nutrient deprivation on agar plates induced by high cell density triggers strong cell aggregation in cells lacking V-ATPase activity. This effect could be caused by increased cell-cell and cell-substratum adhesion and would explain the hyperinvasive phenotype of the *vma* mutants. In line with this model, the morphology of *vma2*Δ, *vma3*Δ, and *vma13*Δ cells was indistinguishable from that of the wild type (Fig. 5E). Thus, it seems that the observed increase in agar invasion is not caused by stronger cell elongation, but rather, by a change in adhesion.

Next, we characterized the link between *VMA13* and known components of signaling pathways for agar invasion. Deletion of either *STE20* or *TPK2*, the activating catalytic PKA subunit gene in filamentous growth, resulted in a strong invasive-growth defect (Fig. 6A). In the *ste20*Δ *tpk2*Δ strain, agar invasion was completely abolished (Fig. 6A), suggesting that the Ste20 and PKA pathways are the major signaling cascades in filamentation, which is in line with observations of other groups (30, 39, 49, 50) (Fig. 1). Interestingly, *VMA13* deletion suppressed the invasive-growth defect of *ste20*Δ cells (Fig. 6A). The agar invasion defect of *ste20*Δ cells can also be suppressed by deletion of either *VMA2* or *VMA3* (Fig. 6B), indicating that loss of V-ATPase activity, not absence of a specific subunit, triggers the underlying signaling pathways. This invasion is possibly mediated by activation of the PKA pathway. *VMA13* deletion also rescued the agar invasion defect of the *tpk2*Δ strain (Fig. 6A), where invasion might be induced by activation of the Ste20-driven MAPK pathway. Notably, the *vma13*Δ *ste20*Δ *tpk2*Δ triple mutant did not exhibit any invasive growth (Fig. 6A). Together, these data suggest that loss of V-ATPase activity can trigger agar invasion by activating both the Ste20 and PKA pathways.

Because of the interactions between Ste20 and the V-ATPase described above and the fact that both proteins are involved in invasive growth, we speculated that Ste20 and the V-ATPase may be parts of a novel pathway regulating filamentation. The only known function of Ste20 in filamentous growth is the activation of

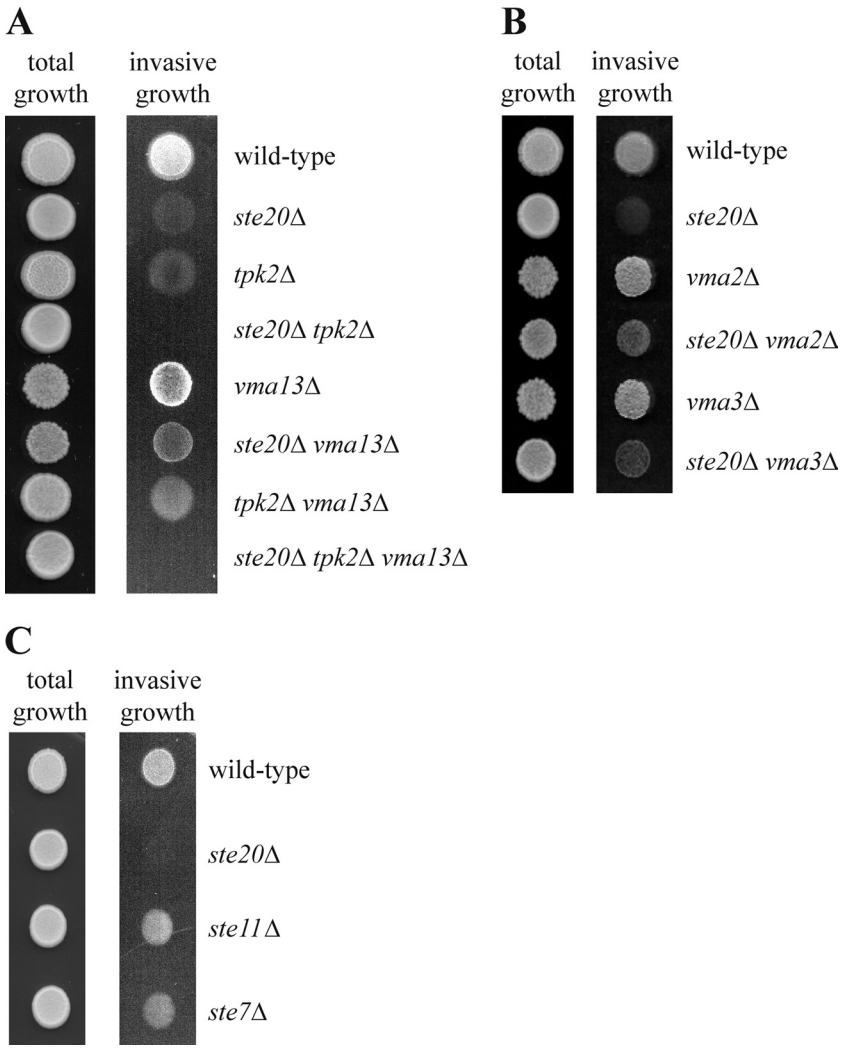

FIG 6 PKA and MAPK signaling in *vma13*Δ cells. (A) *VMA13* deletion leads to activation of the Ste20 and PKA pathways. Agar invasion by the indicated strains was determined as described in the legend to Fig. 5A. (B) Deletion of either *VMA2* or *VMA3* partially suppresses the agar invasion defect of *ste20*Δ cells. The experiment was performed as described in the legend to Fig. 5A. (C) Deletion of *STE11* or *STE7* results in only a moderate filamentation defect. Agar invasion was determined as described in the legend to Fig. 5A.

a MAPK cascade by phosphorylation of the MAPK kinase kinase Ste11 (30, 49, 62, 64). We reasoned that if Ste11 were the only Ste20 target, deletion of *STE11* would cause a defect in filamentous growth as severe as that observed in the *ste20*Δ strain. Importantly, the agar invasion phenotype of *ste11*Δ cells was much less pronounced than that of cells lacking *STE20* (Fig. 6C). Deletion of *STE7*, which encodes the MAPK kinase that is activated by Ste11 during filamentous growth, similarly led to only a relatively moderate phenotype (Fig. 6C). Ste20 also activates Ste11 and Ste7 during mating. Notably, all three *STE* genes are essential for this process (data not shown) (14, 26). Thus, the difference in phenotype severity between the *ste* mutants is specific for filamentous growth and could be explained by additional functional targets of Ste20, such as the V-ATPase. This is in line with the regulation of V-ATPase activity by Ste20 as described above.

DISCUSSION

Regulation of V-ATPase activity by Ste20. The Cdc42 effector Ste20 is involved in multiple signaling pathways, including a MAPK cascade that triggers filamentation (30, 49). Here, using the split-ubiquitin technique, a pulldown assay, and coimmunoprecipitation, we showed that Ste20 specifically interacts with the V-ATPase subunit Vma13, demonstrating that these proteins bind to each other *in vivo* and *in vitro*. We further reported the stimulation of V-ATPase activity by Ste20. It is not clear how Ste20 regulates V-ATPase activity. V_0-V_1 assembly, a major control mechanism, is not affected by overexpression or deletion of *STE20*. Vma13, which activates the assembled V-ATPase (15), does not seem to be a phosphorylation target of Ste20. V-ATPase activation by Ste20 requires Ste20 kinase activity, but Vma13 was not phosphorylated in our hands. Therefore, other V-ATPase subunits might be targets of Ste20, with Vma13 serving as a platform for binding.

Ste20 has previously been known to localize to the plasma membrane at sites of polarized growth in the cytoplasm and the nucleus (1, 25, 28, 43). Here, we show that Ste20 is also enriched in vacuolar membranes. This localization of Ste20 is in line with its

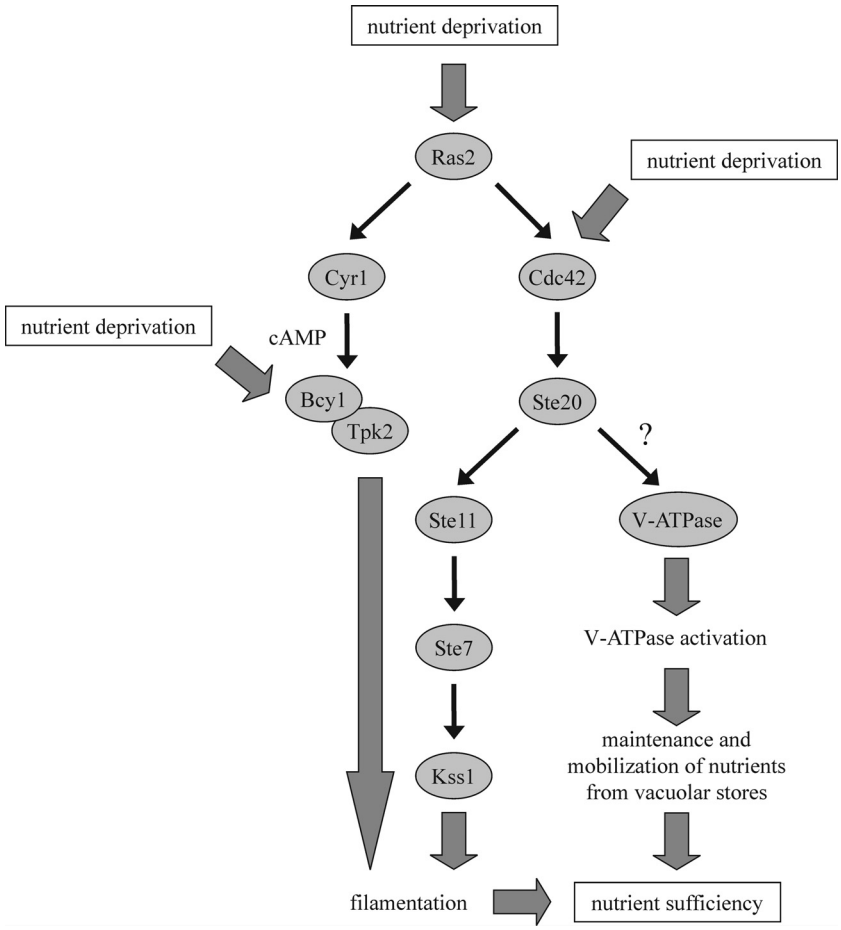

FIG 7 Model of Ste20 and Vma13 functions during filamentous growth. Low nutrient levels in cells growing on a solid surface trigger the PKA and filamentous-growth MAPK pathways. This results in cell elongation, increased adhesion, and growth into the substratum. We propose that, in addition to these signaling events, Ste20 activates V-ATPase, possibly via Vma13. This leads to a lower vacuolar pH, allowing optimal storage and mobilization of nutrients that are required for cell growth. Therefore, filamentous growth and allocation of nutrients complement each other.

role in V-ATPase activation and is consistent with observations of other groups. Cdc42 and Bem1, a scaffold protein that brings Cdc42, its activator Cdc24, and Ste20 into close proximity, are also present at vacuolar membranes (9, 10, 37, 46, 66). Thus, it seems that not only Ste20 associates with vacuolar membranes, but all components of the Bem1-Cdc24-Cdc42-Ste20 cascade.

It has been reported that, together with Cla4, another Cdc42 effector and also a p21-activated kinase, Ste20 regulates vacuolar inheritance (2). Thus, Ste20 has at least two distinct vacuolar functions.

Hyperinvasive growth is stimulated in the absence of V-ATPase activity. Deletion of a number of V-ATPase subunits leads to strongly increased invasive growth relative to wild-type cells. This phenotype is not caused by increased cell elongation. Instead, it correlates with strong cell clustering. *vma* mutants probably experience acute nutrient deprivation under conditions where wild-type cells remain nutrient replete. The vacuolar pH gradient is required for both uptake and mobilization of nutrients (27, 51). The loss of vacuolar acidification in *vma* mutants causes defective nutrient storage and mobilization in these strains (54). Since depletion of certain nutrients induces filamentation, it seems most likely that the hyperinvasive phenotype of *vma* mutants is caused by the failure of these cells to maintain sufficient nutrient stores for times of starvation. As a consequence, cells lacking V-ATPase activity would be much more sensitive to nutrient limitation. Stronger invasive growth might increase the chance of finding extracellular nutrients and would therefore be beneficial for these cells.

Our genetic data suggest that *STE20* and *TPK2* are both required for the hyperinvasive phenotype of *vma13*Δ cells, but it is not clear how a nutrient deprivation signal activates these pathways. This is most likely an intracellular signal. Possibly, cells are able to somehow sense the loss of nutrient storage, as suggested for autophagy-deficient yeast (34). In fact, a direct role for the V-ATPase in lysosomal amino acid sensing by mTORC1 in mammals was recently described (70), although this pathway involves Ragulator components not present in yeast. Alternatively, since the V-ATPase plays a crucial role in the homeostasis not only of vacuolar but also of cytosolic pH (35), the altered pH of these compartments may trigger filamentation.

The only function that has been attributed to Ste20 in filamentous growth is the phosphorylation and thereby activation of the MAPK kinase kinase Ste11 (30, 49, 62, 64) (Fig. 7). In this work, we show that *ste11*Δ and *ste7*Δ cells exhibit a rather mild invasive-

growth defect. In contrast, in cells lacking *STE20*, agar invasion is almost completely absent. This difference in phenotype severity is filamentation specific. *STE20*, *STE11*, and *STE7* are all absolutely required for mating (14, 26). A likely explanation for the more pronounced phenotype of *ste20*Δ cells is that Ste20 has targets beyond Ste11 in filamentous growth. Here, we show that Ste20 can activate V-ATPase activity. Although this observation was obtained in yeast cells grown in nutrient-replete liquid medium, activation of the V-ATPase by Ste20 could be particularly important for filamentous growth on solid surfaces (Fig. 7). When nutrients are limited in cells growing on a solid surface, Ste20 triggers the Ste11-Ste7-Kss1 cascade. Together with other activated pathways, including PKA, this results in cell elongation, substratum invasion, and increased adhesion. Under these conditions, Ste20 could stimulate V-ATPase activity as well, sustaining vacuolar pH gradients during nutrient mobilization by vacuolar antiporters and allowing more efficient mobilization of intracellular reserves required for cell elongation. Thus, filamentous growth and vacuolar mobilization are complementary approaches to deal with starvation. Unfortunately, altered V-ATPase activity during true filamentous growth cannot easily be examined because the cells grow into the agar, precluding biochemical isolation of vacuoles.

Low glucose levels induce filamentation and also trigger disassembly and downregulation of V-ATPase (4, 6, 20). Here, we propose that V-ATPase activity might be increased during filamentous growth. These seemingly contradictory observations can be reconciled. The experiments demonstrating V-ATPase disassembly in response to glucose depletion were carried out in liquid medium (6, 20). Under these conditions, it is likely to be advantageous to reduce growth and to save energy by V-ATPase disassembly. In contrast, for cells growing on a solid medium it may become essential to increase V-ATPase activity and to invade the substratum because there is a chance of finding nutrients. Disassembly of the V-ATPase in response to glucose deprivation is suppressed at high extracellular pH (8), presumably in order to preserve organelle acidification under conditions of alkaline stress. Similarly, nutrient limitation under filamentous-growth conditions may prevent disassembly so that high V-ATPase activity can be maintained.

We found that *STE20* deletion specifically exacerbates the growth defect of *vma13*Δ cells. This observation is somewhat puzzling, since mutations in V-ATPase subunits abolish all V-ATPase activity and generally result in similar growth phenotypes, and it is unlikely that Vma13 functions outside the V-ATPase. Vma13 does play a distinctive role in regulating V-ATPase activity, however, acting as an inhibitor of ATPase activity in cytosolic V_1 complexes but as an activator of the intact V-ATPase (41). Because of this regulatory role, *vma13*Δ mutations show very specific genetic interactions with certain other *vma* mutations (47), and the genetic interaction with *ste20*Δ observed here could also be accounted for by an increased need for the silencing or activating properties of Vma13 in this mutant. Further investigation will be necessary to test this possibility.

In summary, we describe a link between V-ATPase and invasive growth and demonstrate the activation of V-ATPase activity by Ste20. Since these components are conserved from yeast to humans, it will be interesting to test whether V-ATPase activity is modulated in a similar way in higher eukaryotes.

ACKNOWLEDGMENTS

We thank Silke Horn, Maureen Tarsio, and Theodore Diakov for excellent technical support.

The project was supported by Deutsche Forschungsgemeinschaft grant HO 2098/3 to T.H. and NIH grant R01 GM50322 to P.M.K.

REFERENCES

1. **Ahn SH, et al.** 2005. Sterile 20 kinase phosphorylates histone H2B at serine 10 during hydrogen peroxide-induced apoptosis in *S. cerevisiae.* Cell **120**:25–36.
2. **Bartholomew CR, Hardy CF.** 2009. p21-activated kinases Cla4 and Ste20 regulate vacuole inheritance in *Saccharomyces cerevisiae.* Eukaryot. Cell **8**:560–572.
3. **Bond S, Forgac M.** 2008. The Ras/cAMP/protein kinase A pathway regulates glucose-dependent assembly of the vacuolar (H^+)-ATPase in yeast. J. Biol. Chem. **283**:36513–36521.
4. **Cullen PJ, Sprague GF.** 2000. Glucose depletion causes haploid invasive growth in yeast. Proc. Natl. Acad. Sci. U. S. A. **97**:13619–13624.
5. **Cullen PJ, et al.** 2004. A signaling mucin at the head of the Cdc42- and MAPK-dependent filamentous growth pathway in yeast. Genes Dev. **18**: 1695–1708.
6. **Dechant R, et al.** 2010. Cytosolic pH is a second messenger for glucose and regulates the PKA pathway through V-ATPase. EMBO J. **29**:2515–2526.
7. **Diab H, Ohira M, Liu M, Cobb E, Kane PM.** 2009. Subunit interactions and requirements for inhibition of the yeast V_1-ATPase. J. Biol. Chem. **284**:13316–13325.
8. **Diakov TT, Kane PM.** 2010. Regulation of vacuolar proton-translocating ATPase activity and assembly by extracellular pH. J. Biol. Chem. **285**: 23771–23778.
9. **Eitzen G, Wang L, Thorngren N, Wickner W.** 2002. Remodeling of organelle-bound actin is required for yeast vacuole fusion. J. Cell Biol. **158**:669–679.
10. **Eitzen G, Thorngren N, Wickner W.** 2001. Rho1p and Cdc42p act after Ypt7p to regulate vacuole docking. EMBO J. **20**:5650–5656.
11. **Etienne-Manneville S.** 2004. Cdc42—the centre of polarity. J. Cell Sci. **117**:1291–1300.
12. **Forgac M.** 2007. Vacuolar ATPases: rotary proton pumps in physiology and pathophysiology. Nat. Rev. Mol. Cell Biol. **8**:917–929.
13. **Gimeno CJ, Ljungdahl PO, Styles CA, Fink GR.** 1992. Unipolar cell divisions in the yeast *S. cerevisiae* lead to filamentous growth: regulation by starvation and RAS. Cell **68**:1077–1090.
14. **Hartwell LH.** 1980. Mutants of *Saccharomyces cerevisiae* unresponsive to cell division control by polypeptide mating hormone. J. Cell Biol. **85**:811–822.
15. **Ho MN, et al.** 1993. VMA13 encodes a 54-kDa vacuolar H^+-ATPase subunit required for activity but not assembly of the enzyme complex in *Saccharomyces cerevisiae.* J. Biol. Chem. **268**:18286–18292.
16. **Höfken T, Schiebel E.** 2002. A role for cell polarity proteins in mitotic exit. EMBO J. **21**:4851–4862.
17. **Jaffe AB, Hall A.** 2005. Rho GTPases: biochemistry and biology. Annu. Rev. Cell Dev. Biol. **21**:247–269.
18. **Janke C, et al.** 2004. A versatile toolbox for PCR-based tagging of yeast genes: new fluorescent proteins, more markers and promoter substitution cassettes. Yeast **21**:947–962.
19. **Johnsson N, Varshavsky A.** 1994. Split ubiquitin as a sensor of protein interactions in vivo. Proc. Natl. Acad. Sci. U. S. A. **91**:10340–10344.
20. **Kane PM.** 1995. Disassembly and reassembly of the yeast vacuolar H^+-ATPase in vivo. J. Biol. Chem. **270**:17025–17032.
21. **Kane PM.** 2006. The where, when, and how of organelle acidification by the yeast vacuolar H^+-ATPase. Microbiol. Mol. Biol. Rev. **70**:177–191.
22. **Kane PM, Kuehn MC, Howald-Stevenson I, Stevens TH.** 1992. Assembly and tareting of peripheral and integral membrane subunits of the yeast vacuolar H^+-ATPase. J. Biol. Chem. **267**:447–454.
23. **Krebs M, et al.** 2010. *Arabidopsis* V-ATPase activity at the tonoplast is required for efficient nutrient storage but not for sodium accumulation. Proc. Natl. Acad. Sci. U. S. A. **107**:3251–3256.
24. **Kuchin S, Vyas VK, Carlson M.** 2002. Snf1 protein kinase and the repressors Nrg1 and Nrg2 regulate *FLO11*, haploid invasive growth, and diploid pseudohyphal differentiation. Mol. Cell. Biol. **22**:3994–4000.
25. **Leberer E, et al.** 1997. Functional characterization of the Cdc42p binding domain of yeast Ste20p protein kinase. EMBO J. **16**:83–97.

26. **Leberer E, Dignard D, Harcus D, Thomas DY, Whiteway M.** 1992. The protein kinase homologue Ste20p is required to link the yeast pheromone response G-protein $\beta\gamma$ subunits to downstream signalling components. EMBO J. **11**:4815–4824.
27. **Li SC, Kane PM.** 2009. The yeast lysosome-like vacuole: endpoint and crossroads. Biochim. Biophys. Acta **1793**:650–663.
28. **Lin M, et al.** 2009. The Cdc42 effectors Ste20, Cla4 and Skm1 down-regulate the expression of genes involved in sterol uptake by a MAPK-independent pathway. Mol. Biol. Cell **20**:4826–4837.
29. **Lin M, Grillitsch K, Daum G, Just U, Höfken T.** 2009. Modulation of sterol homeostasis by the Cdc42p effectors Cla4p and Ste20p in the yeast *Saccharomyces cerevisiae.* FEBS J. **276**:7253–7264.
30. **Liu H, Styles CA, Fink GR.** 1993. Elements of the yeast pheromone response pathway required for filamentous growth of diploids. Science **262**:1741–1744.
31. **Longtine MS, et al.** 1998. Additional modules for versatile and economical PCR-based gene deletion and modification in *Saccharomyces cerevisiae.* Yeast **14**:953–961.
32. **Lu M, Sautin YY, Holliday LS, Gluck SL.** 2004. The glycolytic enzyme aldolase mediates assembly, expression, and activity of vacuolar H^+-ATPase. J. Biol. Chem. **279**:8732–8739.
33. **Lu A, Hirsch JP.** 2005. Cyclic AMP-independent regulation of protein kinase A substrate phosphorylation by Kelch repeat proteins. Eukaryot. Cell **4**:1794–1800.
34. **Ma J, et al.** 2007. An interrelationship between autophagy and filamentous growth in budding yeast. Genetics **177**:205–214.
35. **Martínez-Muñoz GA, Kane P.** 2008. Vacuolar and plasma membrane proton pumps collaborate to achieve cytosolic pH homeostasis in yeast. J. Biol. Chem. **283**:20309–20319.
36. **Mösch HU, Roberts RL, Fink GR.** 1996. Ras2 signals via the Cdc42/Ste20/mitogen-activated protein kinase module to induce filamentous growth in *Saccharomyces cerevisiae.* Proc. Natl. Acad. Sci. U. S. A. **93**:5352–5356.
37. **Müller O, Johnson DI, Mayer A.** 2001. Cdc42p functions at the docking stage of yeast vacuole membrane fusion. EMBO J. **20**:5657–5665.
38. **O'Rourke SM, Herskowitz I.** 1998. The Hog1 MAPK prevents cross talk between the HOG and pheromone response MAPK pathways in *Saccharomyces cerevisiae.* Genes Dev. **12**:2874–2886.
39. **Pan X, Heitman J.** 1999. Cyclic AMP-dependent protein kinase regulates pseudohyphal differentiation in *Saccharomyces cerevisiae.* Mol. Cell. Biol. **19**:4874–4887.
40. **Park HO, Bi E.** 2007. Central roles of small GTPases in the development of cell polarity in yeast and beyond. Microbiol. Mol. Biol. Rev. **71**:48–96.
41. **Parra KJ, Keenan KL, Kane PM.** 2000. The H subunit (Vma13p) of the yeast V-ATPase inhibits the ATPase activity of cytosolic V1 complexes. J. Biol. Chem. **275**:21761–21767.
42. **Peeters T, et al.** 2006. Kelch-repeat proteins interacting with the Galpha protein Gpa2 bypass adenylate cyclase for direct regulation of protein kinase A in yeast. Proc. Natl. Acad. Sci. U. S. A. **103**:13034–13039.
43. **Peter M, Neiman AM, Park HO, van Lohuizen M, Herskowitz I.** 1996. Functional analysis of the interaction between the small GTP binding protein Cdc42 and the Ste20 protein kinase in yeast. EMBO J. **15**:7046–7059.
44. **Raitt DC, Posas F, Saito H.** 2000. Yeast Cdc42 GTPase and Ste20 PAK-like kinase regulate Sho1-dependent activation of the Hog1 MAPK pathway. EMBO J. **19**:4623–4631.
45. **Ramer SW, Davis RW.** 1993. A dominant truncation allele identifies a gene, *STE20*, that encodes a putative protein kinase necessary for mating in *Saccharomyces cerevisiae.* Proc. Natl. Acad. Sci. U. S. A. **90**:452–456.
46. **Richman TJ, Sawyer MM, Johnson DI.** 2002. *Saccharomyces cerevisiae* Cdc42p localizes to cellular membranes and clusters at sites of polarized growth. Eukaryot. Cell **1**:458–468.
47. **Rizzo JM, Tarsio M, Martinez-Munoz GA, Kane PM.** 2007. Diploids heterozygous for a *vma13*Δ mutation in *Saccharomyces cerevisiae* highlight the importance of V-ATPase subunit balance in supporting vacuolar acidification and silencing cytosolic V_1-ATPase activity. J. Biol. Chem. **282**:8521–8532.
48. **Roberts CJ, Raymond CK, Yamashiro CT, Stevens TH.** 1991. Methods for studying the yeast vacuole. Methods Enzymol. **194**:644–661.
49. **Roberts RL, Fink GR.** 1994. Elements of a single MAP kinase cascade in *Saccharomyces cerevisiae* mediate two developmental programs in the same cell type: mating and invasive growth. Genes Dev. **8**:2974–2985.
50. **Robertson LS, Fink GR.** 1998. The three yeast A kinases have specific signaling functions in pseudohyphal growth. Proc. Natl. Acad. Sci. U. S. A. **95**:13783–13787.
51. **Russnak R, Konczal D, McIntire SL.** 2001. A family of yeast proteins mediating bidirectional vacuolar amino acid transport. J. Biol. Chem. **276**:23849–23857.
52. **Seol JH, Shevchenko A, Shevchenko A, Deshaies RJ.** 2001. Skp1 forms multiple protein complexes, including RAVE, a regulator of V-ATPase assembly. Nat. Cell Biol. **3**:384–391.
53. **Sheu YJ, Barral Y, Snyder M.** 2000. Polarized growth controls cell shape and bipolar bud site selection in *Saccharomyces cerevisiae.* Mol. Cell. Biol. **20**:5235–5247.
54. **Shimazu M, Sekito T, Akiyama K, Ohsumi Y, Kakinuma Y.** 2005. A family of basic amino acid transporters of the vacuolar membrane from *Saccharomyces cerevisiae.* J. Biol. Chem. **280**:4850–4857.
55. **Smardon AM, Tarsio M, Kane PM.** 2002. The RAVE complex is essential for stable assembly of the yeast V-ATPase. J. Biol. Chem. **277**:13831–13839.
56. **Smardon AM, Kane PM.** 2007. RAVE is essential for the efficient assembly of the C subunit with the vacuolar H^+-ATPase. J. Biol. Chem. **282**:26185–26194.
57. **Tiedje C, Holland DG, Just U, Höfken T.** 2007. Proteins involved in sterol synthesis interact with Ste20 and regulate cell polarity. J. Cell Sci. **120**:3613–3624.
58. **Tiedje C, Sakwa I, Just U, Höfken T.** 2008. The Rho GDI Rdi1 regulates Rho GTPases by distinct mechanisms. Mol. Biol. Cell **19**:2885–2896.
59. **Toda T, et al.** 1985. In yeast, RAS proteins are controlling elements of adenylate cyclase. Cell **40**:27–36.
60. **Toda T, et al.** 1987. Cloning and characterization of *BCY1*, a locus encoding a regulatory subunit of the cyclic AMP-dependent protein kinase in *Saccharomyces cerevisiae.* Mol. Cell. Biol. **7**:1371–1377.
61. **Toda T, Cameron S, Sass P, Zoller M, Wigler M.** 1987. Three different genes in *S. cerevisiae* encode the catalytic subunits of the cAMP-dependent protein kinase. Cell **50**:277–287.
62. **van Drogen F, et al.** 2000. Phosphorylation of the MEKK Ste11p by the PAK-like kinase Ste20p is required for MAP kinase signaling in vivo. Curr. Biol. **10**:630–639.
63. **Wittke S, Lewke N, Müller S, Johnsson N.** 1999. Probing the molecular environment of membrane proteins in vivo. Mol. Biol. Cell **10**:2519–2530.
64. **Wu C, Whiteway M, Thomas DY, Leberer E.** 1995. Molecular characterization of Ste20p, a potential mitogen-activated protein or extracellular signal-regulated kinase kinase (MEK) kinase kinase from *Saccharomyces cerevisiae.* J. Biol. Chem. **270**:15984–15992.
65. **Xue Y, Batlle M, Hirsch JP.** 1998. GPR1 encodes a putative G protein-coupled receptor that associates with the Gpa2p Galpha subunit and functions in a Ras-independent pathway. EMBO J. **17**:1996–2007.
66. **Xu H, Wickner W.** 2006. Bem1p is a positive regulator of the homotypic fusion of yeast vacuoles. J. Biol. Chem. **281**:27158–27166.
67. **Yang Z, Huang J, Geng J, Nair U, Klionsky DJ.** 2006. Atg22 recycles amino acids to link the degradative and recycling functions of autophagy. Mol. Biol. Cell **17**:5094–5104.
68. **Yoon JH, Choi EJ, Parker R.** 2010. Dcp2 phosphorylation by Ste20 modulates stress granule assembly and mRNA decay in *Saccharomyces cerevisiae.* J. Cell Biol. **189**:813–827.
69. **Zhang J, Myers M, Forgac M.** 1992. Characterization of the V_0 domain of the coated vesicle (H^+)-ATPase. J. Biol. Chem. **267**:9773–9778.
70. **Zoncu R, et al.** 2011. mTORC1 senses lysosomal amino acids through an inside-out mechanism that requires the vacuolar H^+-ATPase. Science **334**:678–683.